LBL-22110
c.2

LBL-22110
Preprint

RECEIVED
LAWRENCE
BERKELEY LABORATORY

DEC 23 1986

LIBRARY AND
DOCUMENTS SECTION

Submitted to Physical Review

THE EFFECT OF UNIAXIAL STRESS ON IRON-BORON AND IRON-ALUMINUM DEFECTS IN SILICON

D.D. Nolte, E.E. Haller,
L.M. Falicov, and P. Omling

October 1986

TWO-WEEK LOAN COPY

This is a Library Circulating Copy which may be borrowed for two weeks.

Lawrence Berkeley Laboratory
University of California
Berkeley, California 94720

Prepared for the U.S. Department of Energy
under Contract DE-AC03-76SF00098

Center for Advanced Materials

LBL-22110
c.2

DISCLAIMER

This document was prepared as an account of work sponsored by the United States Government. While this document is believed to contain correct information, neither the United States Government nor any agency thereof, nor the Regents of the University of California, nor any of their employees, makes any warranty, express or implied, or assumes any legal responsibility for the accuracy, completeness, or usefulness of any information, apparatus, product, or process disclosed, or represents that its use would not infringe privately owned rights. Reference herein to any specific commercial product, process, or service by its trade name, trademark, manufacturer, or otherwise, does not necessarily constitute or imply its endorsement, recommendation, or favoring by the United States Government or any agency thereof, or the Regents of the University of California. The views and opinions of authors expressed herein do not necessarily state or reflect those of the United States Government or any agency thereof or the Regents of the University of California.

The effect of uniaxial stress on iron-boron and iron-aluminum defects in silicon

D.D. Nolte*, E.E. Haller†, L. M. Falicov*

Lawrence Berkeley Laboratory

*Department of Physics

and †Department of Materials Science and Mineral Engineering,

University of California, Berkeley, California 94720

and

P. Omling

Department of Solid State Physics, University of Lund

P.O. Box 118, S-221 00 Lund, Sweden

ABSTRACT

Deep Level Transient Spectroscopy (DLTS) under uniaxial stress has been applied to the iron-boron impurity level at E_v + 100 meV in silicon, and to both iron-aluminum levels in silicon at E_v + 130 meV and E_v + 200 meV respectively. Although splittings of the DLTS peaks were observed, large, anisotropic shifts in the peak temperatures occurred. The thermal emission of carriers to a stress-split valence band was used to fit the energy of the defect under uniaxial compression. Although these centers exhibit axial symmetry in electron paramagnetic resonance (EPR), the stress anisotropy suggests that, at the elevated temperatures of DLTS, the defects reorient under applied stress. The symmetry of these systems is consistent with that of a freely (or only slightly hindered) reorienting electric dipole in a tetrahedral-strain field.

I. INTRODUCTION

Iron-boron pairs are the dominant defects present in Si:B following iron diffusion and quenching. They constitute part of a larger class of iron-acceptor pairs including FeAl, FeGa, and FeIn. The pairing reaction occurs only in p-type material in which the Fermi energy lies in the lower half of the band gap. For this position of the Fermi level, both the iron and the acceptor are ionized with opposite charges. The resulting coulomb attraction between the ionized donor and acceptor provides the mechanism for the capture of the mobile interstitial iron by the substitutional Group III element.

Iron-acceptor pairs in silicon were first detected by Ludwig and Woodbury[1] using electron paramagnetic resonance (EPR). The defects were found to be highly anisotropic and to exhibit trigonal symmetry, except for FeIn which exhibited orthorhombic C_{2v} symmetry (ordinarily called rhombic I). Recently, a rhombic I configuration has also been identified[2] for FeAl using EPR. Detailed EPR studies of FeB pairs in silicon have been carried out independently by Gehlhof and Segsa[3] and van Kooten et al.[2] Gehlhof and Segsa considered a four-fold multiplet for their ground state and included zero-field splitting to describe the anisotropy, while van Kooten et al. considered only a spin doublet in their analysis and included the anisotropy in their g-tensor. Both arrived at a strong repulsive trigonal field for FeB. On physical grounds the trigonal field would be expected to be strongly repulsive because of the negative charge of the boron. The previously accepted model for the iron-acceptor pair (derived exclusively from the EPR data) places the iron in the tetrahedral interstitial site adjacent to the substitutional site in the trigonal

centers (2.43 Å next nearest neighbor separation). In the rhombic I center of FeAl the iron is assumed to be situated in the next nearest neighbor interstitial site (2.74 Å next nearest neighbor separation). Of course, the iron is likely to relax towards the substitutional site because of the attractive coulomb field.

Iron-acceptor pairs in silicon have been studied extensively using Deep Level Transient Spectroscopy (DLTS).[4,5,6] After iron diffusion in silicon a level is observed at E_v + 0.44 eV. This level is assigned to the isolated interstitial iron. An additional level is observed at E_v + 0.10 eV in Si:B after iron diffusion which has been ascribed to the FeB pair. Two defect levels have been observed in Si:Al after iron diffusion, FeAl(2) at E_v + 0.13 eV and FeAl(1) at E_v + 0.20 eV. These have tentatively been identified, respectively, as the rhombic I and trigonal FeAl configurations[7] observed in EPR. A level associated with FeGa pairs is found at E_v + 0.24 eV in Si:Ga.

As proposed by Ludwig and Woodbury[1], the 4s electrons of interstitial transition-metal elements in silicon are not required for bonding and are transferred to the 3d shell. The iron interstitial energy level (E_v + 0.44 eV) is assigned to the first ionization stage of iron, Fe^+/Fe^0, or a $3d^7$-to-$3d^8$ configuration transition. The iron-acceptor pair energy levels, which lie between the interstitial level and the acceptor levels, are considered to involve the second ionization stage of iron, Fe^{++}/Fe^+, with the acceptor remaining ionized and thus negatively charged. This is a $3d^6$-to-$3d^7$ electron configuration transition. The second ionization stage of iron is normally buried deep within the valence band,[8] but the presence of the negatively charged acceptor pushes the energy level up, out of the valence band and into the bandgap by coulomb repulsion[9].

Chantre et. al.[7] have recently demonstrated that the FeAl(2) defect is a metastable state of the FeAl(1) defect. The transformation between the two configurations is controlled by charge state dependences of the total energy. The activation energy for transformation is about 0.5 eV. They further proposed a phenomenological model based solely on coulomb energy which explains the energy difference between the trigonal and rhombic I configurations of FeAl.

Iron-acceptor pairs have also been investigated with photoluminescence. The luminescence from the isoelectronic trap observed in Si:FeIn has been shown to be consistent with a <100> orientation of the constituent atoms,[10] which is also the symmetry observed by EPR for FeIn pairs. An isoelectronic trap observed in Si:FeTl shows similar structure as the FeIn trap,[11] but stress and magnetic field perturbations indicate that the FeTl related trap has <111> axial symmetry.[10] On the other hand, the luminescence from the isoelectronic trap observed in Si:FeB exhibits no axial symmetry under the application of a magnetic field.[12] This lack of orientational splitting of the no-phonon line, along with other less direct evidence,[13] leads to the conclusion that the FeB related defect observed in photoluminescence is not the FeB pair observed in EPR.

It is clear from the foregoing review of the experimental observations of iron-acceptor complexes in silicon that the defects can exhibit a large variety of symmetries: trigonal, rhombic I, and possibly tetrahedral. We chose to investigate the symmetry of the FeB and FeAl defects observed in DLTS by applying uniaxial stress. Hydrostatic experiments have been performed by Wünstel et al.[14] on iron and iron-acceptor pairs using DLTS. They obtain derivatives of the defect energies with respect to hydrostatic pressure of (-11 meV/GPa). Under hydrostatic compression the

iron-acceptor pair energy moves towards the valence band. We applied uniaxial stress to the FeB and FeAl(1) levels observed in DLTS which had been identified as the trigonal defects observed in EPR, and to the FeAl(2) defect which had been assigned rhombic I symmetry. Analysis of our data, together with all other previous results, leads us to the conclusion that the iron-involved pairs behave as easily reorientable dipoles, i. e., as slightly hindered rotators in a tetrahedral crystal-field environment.

In section II we describe the experimental details as well as the stress data and analysis. Possible models of the defect symmetry are discussed in section III and IV.

II. DATA AND ANALYSIS

A. Experimental details

Iron was diffused for two to four hours at 1000°C into 1 mm thick oriented samples of boron or aluminum doped silicon, with shallow compensations in the range of 1 to 5 x 10^{15} cm^{-3}. The samples were quenched in air, then annealed at 80° C for two hours. The quench is necessary to capture the iron as interstitials without precipitation, and the subsequent 80°C annealing stage facilitates the movement of the iron interstitials to speed up their capture by the substitutional boron. The samples were polish-etched and allowed to oxidize before evaporation of the contacts. We evaporated 300 Å of gold onto one surface to form an ohmic contact. The rectifying contact was formed by evaporating 1000 Å of Al onto the opposite side. The evaporation was performed with minimal

power in order to avoid heating of the contact. The aluminum was covered by 300 Å of gold to protect the aluminum from the indium electrical contacts. Typical concentrations of the FeB and FeAl levels after preparation ranged from 5×10^{12} cm^{-3} to 5×10^{13} cm^{-3}.

The stress samples were cut from the prepared sample into 1 mm x 1 mm x 6 mm parallelepipeds. The saw-damaged surface proved to be an excellent electrical insulator and so was retained; however, the ends of the cut samples were etched to remove the sharp edges. We attached 32-gauge magnet wire to the samples using pressed indium contacts. Samples were mounted into a DLTS stress rig capable of achieving 100 kg per mm^2, or 1 GPa of uniaxial stress.

The stress data were taken with the time constant of the DLTS correlator set to a fixed value, usually around 3 ms. Zero-stress data were taken, then the stress was increased by intervals of about 0.1 GPa to nearly 1 GPa. The zero-stress measurement was repeated afterwards to check for stress hysteresis. Data were always taken for increasing temperature under 1/100 atm of helium exchange gas in order to equilibrate the temperatures within the stress rig and remove any effects from thermal hysteresis. A representative example of stress data for FeB is shown in Fig. 1 for increasing stress along a <110> direction at constant emission rate, and for both FeAl defects in Fig. 2 for <100> stress. Two features are evident: first, there are no splittings of the DLTS peaks greater than 3 meV/GPa; second, the peaks shift in temperature by roughly 15 K/GPa. The effect of stress on thermal emission to a split valence band must be considered in order to explain the large observed shifts in temperature of the DLTS peaks and to extract the shift in energies of the defects.

B. Emission Rate to a Stress-Split Valence Band

The four-fold degenerate valence band in silicon splits under stress, upsetting the emission rate analysis derived by detailed balance which assumes an average density of states for the band edge. The band splits into two distinct doublets[15], with different effective masses and hence different density of states and thermal velocities. Under uniaxial stress, τ, the thermal emission rate breaks into two competing contributions: one contribution arising from thermal hole emission to the light-hole band, and the other arising from thermal hole emission to the heavy-hole band. The total thermal emission rate is the sum of the independent rates

$$e(\tau) = c\, T^2 \{ \sigma_L(\tau)\, m^*_L(\tau) \exp[-(E_T(\tau) - E_L(\tau))/kT] + \sigma_H(\tau)\, m^*_H(\tau) \exp[-(E_T(\tau) - E_H(\tau))/kT] \} \quad (1)$$

where H and L refer to the heavy-hole and the light-hole band respectively, $\sigma_L(\tau)$ and $\sigma_H(\tau)$ are the capture cross sections, $m^*_L(\tau)$ and $m^*_H(\tau)$ are the average effective masses, $E_T(\tau)$ is the trap energy, and $E_L(\tau)$ and $E_H(\tau)$ are the band energies.

Because the independent emission rates add to give a single effective emission rate, the capacitive transient consists of a single exponential decay which produces a single DLTS peak. Similarly, formerly degenerate defect levels (split by stress), whose occupancies are related by a Boltzman factor produce a single DLTS peak. The only condition for producing multiple DLTS peaks from a split defect degeneracy requires that the repopulation rate among the defect states must be much slower than

both the thermal emission rate and the rate for a single scan over the DLTS peak. However, if the repopulation rate is much slower than the emission rate, but is still faster than the scan rate, then simple reorientation occurs and there is again only a single DLTS peak corresponding to the lowest energy configuration. Electronic repopulation rates are always much faster than emission rates, therefore the splitting of electronic degeneracy always produces a single DLTS peak. From these considerations the splitting of DLTS peaks under stress is expected to be relatively rare and to occur only for rigid, (i.e., non-reorienting) anisotropic defects.

All of the parameters in (1) can vary as a function of stress. The analysis of the emission rate is facilitated by two factors: first, the energy shifts of the valence band under stress are well known from exciton spectroscopy[16]; and second, the light-hole and heavy-hole effective masses saturate above 0.4 GPa to constant values measured by cyclotron resonance.[17] For these reasons, we only attempt to fit the data for stresses greater than 0.4 GPa. The effect of uniaxial stress on the capture cross sections is not known accurately. Wünstel et al.[14] observed no measurable change in the capture cross section under hydrostatic stress. We measured the capture cross section of FeAl(1) under both zero stress and 0.6 GPa of uniaxial stress and saw no change in the capture cross section within experimental error. The shift in the DLTS peak temperature depends only logarithmically on the capture cross section and on the effective masses, while it depends linearly on the energies, so any small change in these parameters should not introduce significant error into the analysis. Therefore, the fitting procedure is expected to be highly accurate, with the defect energy being the only adjustable

parameter. The error in the energy determination arises predominantly from errors in the applied stress.

C. Data

The FeB, FeAl(1), and FeAl(2) defects were stressed along the three major crystallographic directions: <111>, <110>, and <100>. In Fig. 3, the shift in temperature of the FeB peak for constant emission rate is plotted as a function of stress for these three directions. Points are experimental data, while the solid line is the theoretical fit (for stresses greater than 0.4 GPa) assuming the relevant energy splittings and saturated effective masses of the valence band. The total energy shift of the FeB level is adjusted to fit the data. The shifts in temperature of FeAl(1) are shown in Fig. 4, and the shifts of FeAl(2) are shown in Fig. 5.

The results of this analysis are summarized in Fig. 6 and Fig. 7, which display the energy shifts under 1 GPa of uniaxial stress. Energy is plotted against stress direction. The origin of energy is taken at the center of gravity of the top of the two valence bands. The zero stress energies of the iron-acceptor pairs are also indicated. There are two contributions to the shift in temperature of the DLTS peak. The predominant contribution stems from the splitting of the valence band. The remaining contribution comes from the total energy shift of the iron-acceptor pair, which can be broken into a hydrostatic component and a shear component. The hydrostatic component is (-3.8 meV/GPa) for FeB, and (-4.0 meV/GPa) for FeAl(1)[14]. The hydrostatic contribution to FeAl(2) has not yet been measured. When these values are subtracted from the total energy shifts of the defects, the shear energy shifts remain. The FeB and

FeAl(1) defects exhibit a strong shear anisotropy of (-2 meV/GPa) in the <111> direction, and nearly equal values of around (-10 meV/GPa) in the <110> and <100> directions. Only the total electronic energy shifts are shown for FeAl(2), since there are no data available on the hydrostatic shift of this defect. However, shear anisotropy is still evident, and is qualitatively similar to the stress behavior of FeB and FeAl(1).

III. DISCUSSION

The two main features of the data are:

1.- For all cases only one signal is obtained. It should be emphasized here that even though excited states of a given defect do not produce a second DLTS signal (as discussed in Section II), defects with different crystal environments do produce different signals. Since only one signal is clearly observed, all defects are equivalent, even under considerable stress. The above arguments lead unquestionably to reorientation of the centers under stress.

2.- The large shifts observed for <100> stresses immediately rule out trigonal defects which give no shear contribution for stress in the <100> directions. The shifts of a trigonal defect are shown in Fig. 8.

In fact, only two possible symmetries are compatible with all our observations: a rhombic I type defect, or a tetrahedral defect with T_2 symmetry. The energy splittings of a rhombic I defect are plotted in Fig. 9 along with the stress data. The parameters $A_1 - (1/3)E_{hydro} = 20$ meV/GPa, $A_2 - (1/3)E_{hydro} = -10$ meV/GPa and $A_3 = 3$ meV/GPa fit the FeB data[18]. In addition, all the rhombic I defects must reorient thermally into the minimum-energy orientation to explain why no orientational

splitting is observed. The energy splittings of a tetrahedral T_2 state are plotted in Fig. 10 along with the stress data. The parameters B = 11 meV/GPa and C = 3 meV/GPa fit the FeB data[19].

Rhombic I symmetry is certainly a plausible symmetry for iron-acceptor pairs because rhombic I centers have already been observed in EPR for one of the FeAl defects and for FeIn. However to assign rhombic symmetry to FeB as well as FeAl(1) and FeAl(2) directly contradicts the results from EPR. Furthermore, most rhombic I defects are strongly anisotropic and would be substantially hindered from reorienting easily within the crystal. A much more natural explanation considers the iron-acceptor pairs as electric dipoles which are freely (or almost freely) rotating in strain-free environments, but which experience a tetrahedral-strain field when an outside stress is applied. This interpretation is still consistent with the data from EPR from which trigonal and rhombic I symmetries are assigned to the defects. It is likely that local potential minima exist in the <111> or <100> directions which have sufficient strength to localize the iron in those minima. But these minima are sufficiently weak so that they do not strongly affect the gross effects of stress on the electronic energies which originate from the dipole character of the centers. In what follows we examine these possibilities.

A. Reorienting rhombic I defect

Because the FeB and FeAl defects are two-center defects, it may seem at first improbable that the defects could have full tetrahedral symmetry. Therefore, the stress data could be explained by assuming that the iron-acceptor pairs are reorienting, high multiplicity defects in which all the centers align in the lowest energy orientation under applied

uniaxial stress. The simplest model for the iron-acceptor system of rhombic I symmetry consists of a substitutional acceptor and an iron nested between a pair of bonds in the <100> directions. The iron could thermally reorient among the six pairs of bonds. The point group for this configuration is C_{2v}. No effects concerning electronic degeneracy need be considered; only orientational splitting followed by reorientation occurs.

There would be two deformation potentials for this defect: Ξ_u and $\Xi_\perp$, defined by

$$\Delta E_u = -1/3 \cdot \Xi_u \cdot (s_{11} - s_{12}) \cdot T,$$

$$|\Delta E_\perp| = 1/2 \cdot \Xi_\perp \cdot s_{44} \cdot T,$$

where s_{11}, s_{12} and s_{44} are the compliance constants and T is the magnitude of uniaxial stress. The first deformation potential is a measure of the interaction energy between the iron and the Group III element. This value is Ξ_u = 3.2 eV ± 1 eV for the FeB defect. The positive value reflects the fact that the potential is repulsive. The second deformation potential is a measure of the interaction energy between the iron and the pair of bonds between which it is situated in the <100> directions. This value is $|\Xi_\perp|$ = 0.3 eV ± 0.3 eV. In a simple point-ion model, the first deformation potential can be related directly to the electrostatic potential energy of the electron in the field of the ionized boron (aluminum). It can be easily shown that $\Xi_u = e^2/\varepsilon d$, where d is the separation between the iron and the acceptor.

For the reasons mentioned above, namely that rhombic I symmetry is unable to provide an explanation for the data reported from EPR and that such anisotropic defects could not reorient easily, we feel that the stress dependence of the iron-acceptor pairs cannot be explained in terms of rhombic I symmetry. On the other hand, both the stress characteristics

and the EPR results can be explained naturally if the pairs are considered to be slightly hindered, rotating electric dipoles.

B. Electric Dipole in a Tetrahedral Environment.

To lowest order, the iron-acceptor pairs can be represented as simple electric dipoles: the iron is positively charged, the boron (aluminum) is negatively charged, and there is some small separation between them. The dipole operator in the tetrahedral group T_d transforms as the T_2 representation of that group, which is a threefold-degenerate representation. The functions (x,y,z) are a basis for the representation and are also components of the dipole (or position) operator. Because all components of the set have equal energy, any linear combination will have the same energy. Therefore, a dipole in a tetrahedral field can orient in any direction with the same total energy, with no potential barriers; the dipole is a free rotator.

When a uniaxial stress field is applied to a dipole in a <u>completely isotropic medium</u>, the dipole reorients to a minimum energy configuration which is independent of stress orientation; the dipole exhibits an isotropic energy shift. When uniaxial stress lowers the symmetry of a tetrahedral environment, on the other hand, a dipole located at the tetrahedral site must exhibit anisotropic energy shifts which depend on the direction of the stress. Specifically, the total energy of the dipole has an angular variation compatible with that of the T_2 symmetry, shown in Fig. 10. The iron-acceptor pairs reorient under applied stress into the plane perpendicular to the stress direction. These perpendicular orientations have the lowest total energy. Under uniaxial stress, the distances parallel to the stress direction are compressed more than the

distances perpendicular to the stress direction by a factor equal to Poisson's ratio. The increase in total energy is therefore greater parallel to the stress than perpendicular, and the defects reorient into the lower-energy perpendicular configurations.

The energies observed by DLTS are electronic energies, not total energies. The electron wave function in the iron d-shell must have an axial symmetry relevant to the instantaneous orientation of the iron within the crystal; in general it should be in an orbital singlet. However the electronic energy does depend on the separation between the iron and the substitutional acceptor, and any change in the separation distance should be observed as a change in the DLTS activation energy. As the total energy of the dipole is changed under application of uniaxial stress, the iron-acceptor separation is altered as well as the orientation of the dipole. Therefore the stress anisotropy of the dipole is reflected in the electronic energy of the defect.

In fact the iron-acceptor pair is not a perfect dipole centered at a tetrahedral site. The spatial extent of the pair, which must conserve its T_2 overall symmetry, causes the defect to experience higher multipole components of the potential which results in a hindered rotator. In general terms, there should be a threshold energy below which the rotator becomes a librator, and the tetrahedral symmetry is then lowered: the isotropy of the system is destroyed. The potential energy must have minima in certain directions, possibly in the <111> or <100> directions. If these minima are shallow, the defect retains much of the stress behavior characteristic of a tetrahedral T_2 state, and at the elevated temperatures of DLTS the defect is still essentially free to reorient. At the low temperatures used in EPR and PL, on the other hand, the iron may

not have enough thermal energy to surmount the potential barriers, and the defect may take on the lower symmetry. The weak crystal field can explain the large variety of symmetries observed by different techniques at different temperatures.

IV. TETRAHEDRAL T_2 STATE WITH SHALLOW TRIGONAL MINIMA

The effect of a tetrahedral crystal field with trigonal or rhombic minima on the stress behavior of a T_2 state can be calculated and used to estimate an upper bound to the strength of the hindering crystal field consistent with the error bars on the stress data. We choose the example of trigonal minima, since it corresponds with the most common iron-acceptor configuration observed by EPR.

A dipole of T_2 symmetry will exhibit four equivalent minima in this case. The librating dipole has A_1 symmetry of the reduced[20] group C_{3v}. There are four distinct such minima corresponding to orientations $[1\bar{1}\bar{1}]$, $[\bar{1}1\bar{1}]$, $[111]$, and $[\bar{1}\bar{1}1]$. The higher energy configurations of that dipole, doubly-degenerate E representations of C_{3v}, should have an energy Δ above A_1, which is a measure of the hindering potential. The Hamiltonians of the four minima for the three principal stress orientations [111], [100] and [110] are given in the Appendix. The results for trigonal minima, with Δ = 30 meV, B = 20 meV/GPa and C = 3 meV/GPa, and stress orientations along the directions $[1\alpha\alpha]$, $[1\alpha 0]$, and $[11\alpha]$, for $0 \leq \alpha \leq 1$, are shown in Fig. 11. There is considerable orientational splitting between the four equivalent orientations. It should be emphasized that Fig. 11 represents the <u>worst</u> possible fit to the

experimental data, compatible with the error bars. Stress data from FeB are included for comparison.

The model, once again, is "acceptable" if reorientation of the defect to its minimum energy configuration is assumed. For trigonal distortions greater than 30 meV, observable differences would appear in the stress behavior. Particularly the free-rotator stress shifts, with their characteristic maxima for <100> stresses, should gradually change into those of a fixed, trigonally oriented defect, with minimum (or zero) shifts for <100> stresses. The two limiting behaviors are given by the lowest-energy curves of Figures 8 and 10. Therefore, experiment proves that the trigonal splitting of the iron-acceptor defects, if any, must be smaller than about 30 meV in order to reproduce the data. This value of the splitting is consistent with our estimated upper bound of about 150 meV for the barrier to reorientation. It is important to note that a 30 meV trigonal splitting effectively localizes the iron in the <111> directions and could provide the trigonal g-tensor observed in EPR. The gross stress behavior, however, would reflect the essentially isotropic origin of the defect.

V. CONCLUSIONS

We have applied uniaxial stress to the FeB, FeAl(1), and FeAl(2) defects and observed considerable shifts but no splitting of the DLTS peaks. All defects showed similar anisotropy in their energy shifts, which are small for <111> stresses and large for <100> stresses.

The lack of splitting in all cases, and the two-center character of the impurity clearly indicates reorienting defects. Stress analysis, in addition, points out to reorientation either to the six equivalent positions of a rhombic I defect, or completely free reorientation to directions determined by the stress. Because trigonal defects have been identified in what we assume are stress-free EPR experiments on both FeAl and FeB centers, it is unlikely that all the defects studied by us are rhombic I. Rhombic I defects in addition tend to be rigid and hard to reorient. We therefore reach the conclusion that all iron-acceptor centers studied here (and possibly others) are in fact almost-free dipole rotators in silicon.

Dipoles are triply degenerate in a tetrahedral field, transforming as the T_2 representation of the tetrahedral group and should show stress dependence compatible with it. In higher order, the real defects are expected to show deviations from isotropic behavior. Energy minima must occur in selected orientations, possibly in either the <111> or <100> directions. The techniques of EPR and PL can resolve energy structure several orders of magnitude smaller than the best DLTS energy resolution. Therefore even relatively small barriers to reorientation of the iron could effectively produce the axial structure observed by EPR and PL. The technique of DLTS, on the other hand, probes a much coarser energy structure of the defect, which originates from the lowest-order dipole nature of the center.

The application of stress in conjunction with EPR would be a critical test of this hypothesis. Two scenarios are possible. If the potential minima are small enough, then the stress field will overwhelm them and the defect should reorient in a direction perpendicular to the applied stress,

transforming the trigonal (or rhombic) defects into a single defect with the symmetry of the strain field. Alternatively, if the potential minima are substantially greater than the largest possible stress field, but if the potential barriers to reorientation are comparable to the thermal energy, then the defect observed in EPR should reorient, while retaining its axial symmetry. In either one of these scenarios only one EPR signal should be observed.

APPENDIX

The matrices of the Hamiltonian for a T_2 ground state split by a trigonal field can be diagonalized by taking the following basis set which is appropriate for the four equivalent <111> orientations:

[111]	[$1\bar{1}\bar{1}$]
A_1: $(1/\sqrt{3})(T_{2,1} + T_{2,2} + T_{2,3})$	A_1: $(1/\sqrt{3})(T_{2,1} - T_{2,2} - T_{2,3})$
E: $(1/\sqrt{2})(T_{2,1} - T_{2,2})$	E: $(1/\sqrt{2})(T_{2,1} + T_{2,2})$
$(1/\sqrt{6})(T_{2,1} + T_{2,2} - 2T_{2,3})$	$(1/\sqrt{6})(T_{2,1} - T_{2,2} + 2T_{2,3})$

[$\bar{1}1\bar{1}$]	[$\bar{1}\bar{1}1$]
A_1: $(1/\sqrt{3})(-T_{2,1} + T_{2,2} - T_{2,3})$	A_1: $(1/\sqrt{3})(-T_{2,1} - T_{2,2} + T_{2,3})$
E: $(1/\sqrt{2})(-T_{2,1} - T_{2,2})$	E: $(1/\sqrt{2})(-T_{2,1} + T_{2,2})$
$(1/\sqrt{6})(-T_{2,1} + T_{2,2} - 2T_{2,3})$	$(1/\sqrt{6})(-T_{2,1} - T_{2,2} - 2T_{2,3})$

where the $T_{2,i}$ are the original tetrahedral T_2 basis components transforming like (x,y,z). The Hamiltonians, including the stress perturbation become:

For [111] stress:

[111] orientation

$$\begin{vmatrix} E_o - \Delta - (2/3)C & 0 & 0 \\ 0 & E_o - (2/3)C & 0 \\ 0 & & E_o + (4/3)C \end{vmatrix}$$

$[1\bar{1}\bar{1}]$, $[\bar{1}1\bar{1}]$, and $[\bar{1}\bar{1}1]$ orientations

$$\begin{vmatrix} E_0 - \Delta - (2/3)C & (4/\sqrt{3}\ 3)C & (-\sqrt{2}/\sqrt{3})\ (2/3)C \\ (4/\sqrt{3}\ 3)C & E_0 - (2/9)C & -\sqrt{2}\ (2/9)C \\ (-\sqrt{2}/\sqrt{3})\ (2/3)C & -\sqrt{2}\ (2/9)C & E_0 - (4/9)C \end{vmatrix}$$

For [100] stress:

All defect orientations

$$\begin{vmatrix} E_0 - \Delta + B/2 & (\sqrt{3}/2)B & (\sqrt{3/2})B \\ (\sqrt{3}/2)B & E_0 - B/2 & B/\sqrt{2} \\ (\sqrt{3/2})B & B/\sqrt{2} & E_0 \end{vmatrix}$$

[110] stress:

$[111]$ and $[1\bar{1}\bar{1}]$ orientations

$$\begin{vmatrix} E_0 - \Delta + B/2 - C & 0 & 0 \\ 0 & E_0 - B/2 + C/3 & B/\sqrt{2} + (\sqrt{2}/3)C \\ 0 & B/\sqrt{2} + (\sqrt{2}/3)C & E_0 + (4/3)C \end{vmatrix}$$

$[1\bar{1}\bar{1}]$ and $[\bar{1}1\bar{1}]$ orientations

$$\begin{vmatrix} E_0 - \Delta + B/2 + C & 0 & 0 \\ 0 & E_0 - B/2 + C/3 & B/\sqrt{2} + (\sqrt{2}/3)C \\ 0 & B/\sqrt{2} + (\sqrt{2}/3)C & E_0 - (4/3)C \end{vmatrix}$$

where Δ is the trigonal field splitting, and B and C are constants defined in Lannoo.[18]

ACKNOWLEDGMENTS

We gratefully acknowledge the many fruitful conversations with W. Walukiewicz, as well as J. Weber and E. Weber. We also thank C.Kisielowski-Kemmerich for providing the aluminum doped material. This work was supported by the Director, Office of Energy Research, Office of Basic Energy Sciences, Materials Science Division of the U.S. Department of Energy under Contract DE-AC03-76SF00098.

REFERENCES

[1]G.W. Ludwig and H.H. Woodbury, Solid State Phys. 13, 223 (2962).

[2]J.J. van Kooten, G.A. Weller, and C.A.J. Ammerlan, Phys. Rev. B30, 4564 (1984).

[3]W. Gehlhof and K.H. Segsa, Phys. Stat. Sol.(b) 115, 443 (1983).

[4]K. Wünstel, K.H. Froehner and P. Wagner, Physica 116B, 301 (1983).

[5]K. Wünstel and P. Wagner, Appl. Phys. A27, 207 (1982).

[6]L.C. Kimerling and J.L. Benton, Physica 116B, 297 (1983)

[7]A. Chantre and D. Bois, Phys. Rev. B 31, 7979 (1985).

[8]A. Zunger, Solid State Physics (1986) (in press).

[9]L. Samuelson and P. Omling, 18th International Conference on the Physics of Semiconductors (1986)

[10]R. Sauer and J. Weber, Physica 116B, 195 (1983).

[11]M.L.W. Thewalt, U.O. Ziemlis, S.P. Watkins, and R.R. Parsons, Can. J. Phys. 60, 1691 (1982).

[12]H.D. Mohring, J. Weber, and R. Sauer, Phys. Rev. B 30, 894 (1984).

[13]T.E. Schlesinger and T.C. McGill, Phys. Rev. B 28, 3643 (1983).

[14]K. Wünstel, O. Kumagai, P. Wagner, and W. Jantsch, Appl. Phys. A 27, 251 (1982).

[15]G.E. Pikus, G.L. Bir, Fizika Tverdogo Tela 11, 1642 (1959).

[16]J. C. Merle, M. Capizzi, P. Fionini, A. Frova, Phys. Rev. B 17, 4821 (1978).

[17]C. Dresselhaus, A.F. Kip, and C. Kittel, Phys. Rev. 98, 368 (1955).

[18]A.A. Kaplyanskii, Opt. Spectro. (USSR) 16, 329 (1964).

[19]M. Lanoo and J. Bourgoin, Point Defects in Semiconductors I, (Springer-Verlag, New York, 1981), p. 29.

[20]The three-dimensional rotator T_2 in tetrahedral symmetry reduces, under C_{3v} symmetry, to a doubly degenerate two-dimensional rotator E and a non-degenerate librator A_1. We take here the symmetry to be that of the librator. Figure 11 includes only the behavior of the four different A_1 levels under stress. The stress separation between the A_1 states of the various orientations is always much smaller than the splitting Δ between A_1 and E.

FIGURE CAPTIONS

Fig. 1 DLTS spectrum of FeB in Si under <110> uniaxial compression. The data were taken for a constant emission time constant τ=3 ms, with the stress varying from zero to 0.76 GPa. The period of each scan was approximately 3 minutes.

Fig. 2 DLTS spectrum of FeAl in Si under <100> uniaxial compression. Data were taken for a constant emission time constant τ=3 ms.

Fig. 3 Shift in the FeB peak temperature for constant emission rate as a function of stress in the (a)<111>, (b)<110>, and (c)<100> directions. The circles are experimental data: solid lines are theoretical fits for the given parameters.

Fig. 4 Shift in the FeAl(1) peak temperature for constant emission rate as a function of stress in the (a)<111>, (b)<110>, and (c)<100> directions.

Fig. 5 Shift in the FeAl(2) peak temperature for constant emission rate as a function of stress in the (a)<111>, (b)<110>, and (c)<100> directions.

Fig. 6 Summary of the energy shifts of FeB under 1 GPa for the three major crystallographic directions. The origin of energy is taken at the center of the valence band. The shifts due to the splitting of the valence band, the hydrostatic shift of the FeB defect, and the shear energy shifts of the FeB defect are all indicated.

Fig. 7 Summary of the energy shifts of FeAl(1) and FeAl(2) under 1 GPa for the three major crystallographic directions.

Fig. 8 Energy shifts of four equivalent trigonal defects under 1 GPa uniaxial stress as functions of stress direction.

Fig. 9 Energy shifts of six equivalent rhombic I defects under 1 GPa uniaxial stress as functions of stress direction.

Fig.10 Energy splittings and shifts of a T_2 level under 1 GPa uniaxial stress as functions of stress direction.

Fig.11 Energy shifts of four equivalent A_1 (C_{3v}) components of a T_2 (T_d) state with a 30 meV trigonal splitting. The four curves represent the iron oriented in the four antibonding <111> directions. The parameters are the worst possible fit to the experimental data, compatible with the error bars.

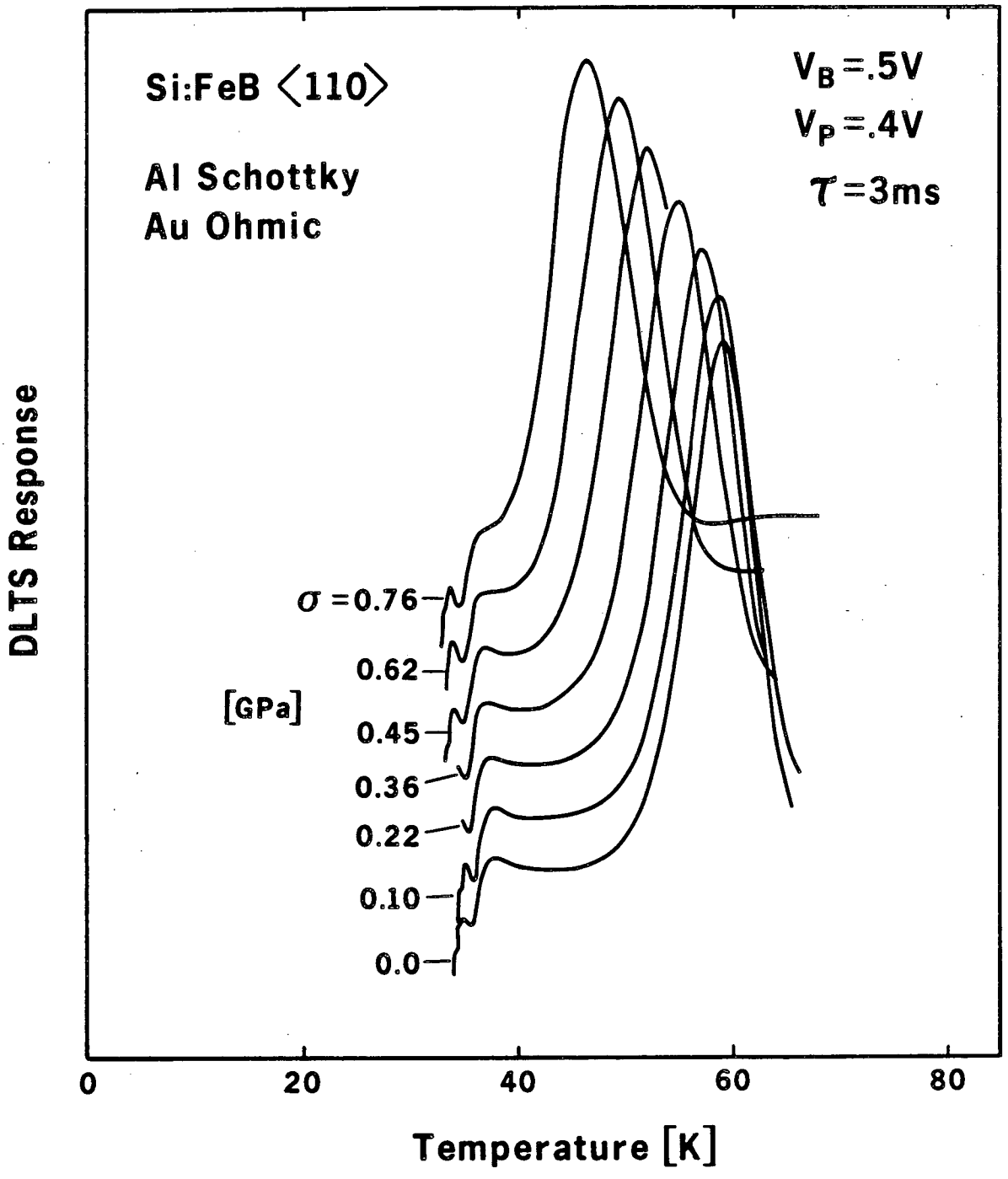

XBL 863-1146

Figure 1.

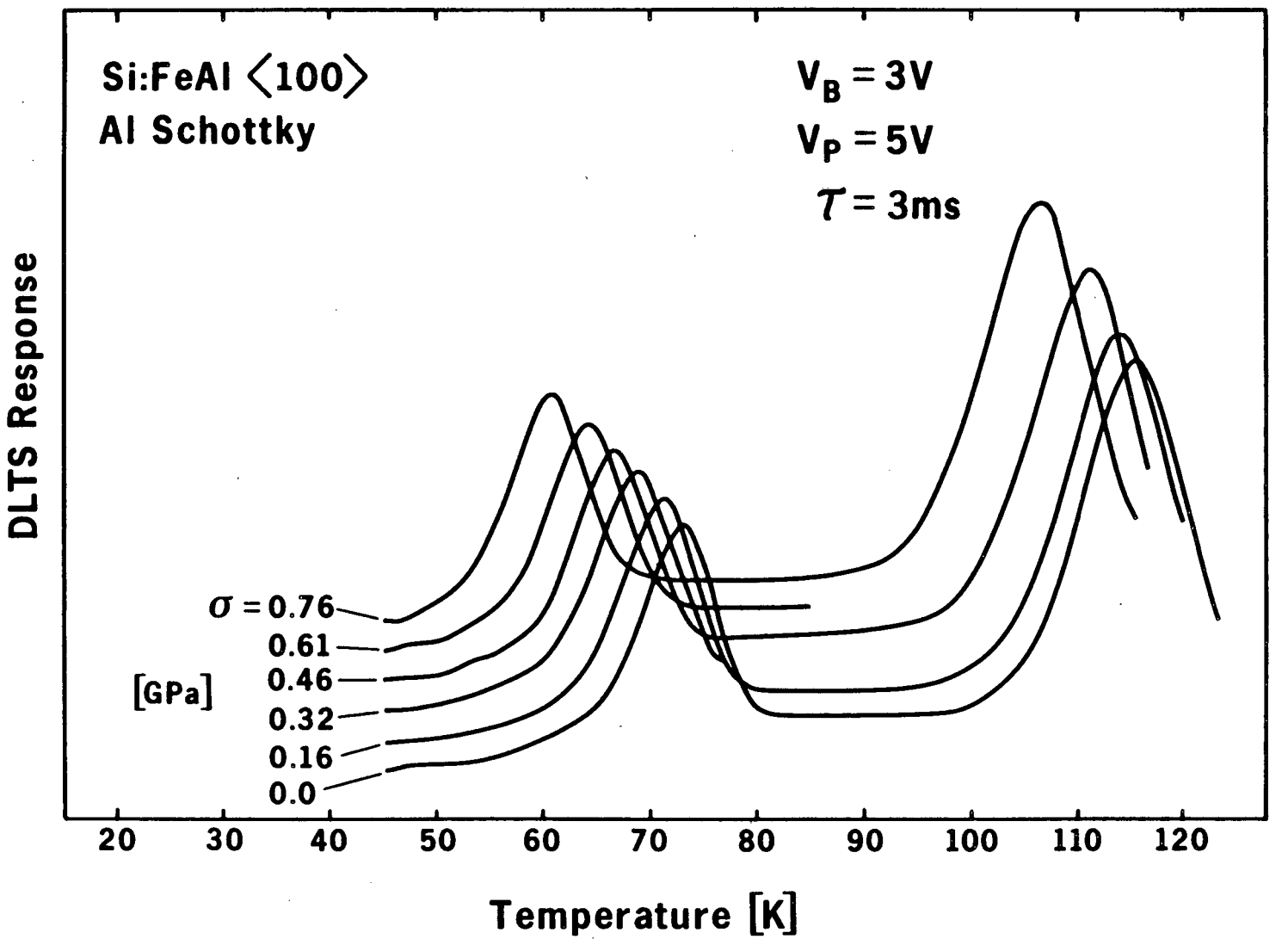

XBL 869-3558

Figure 2.

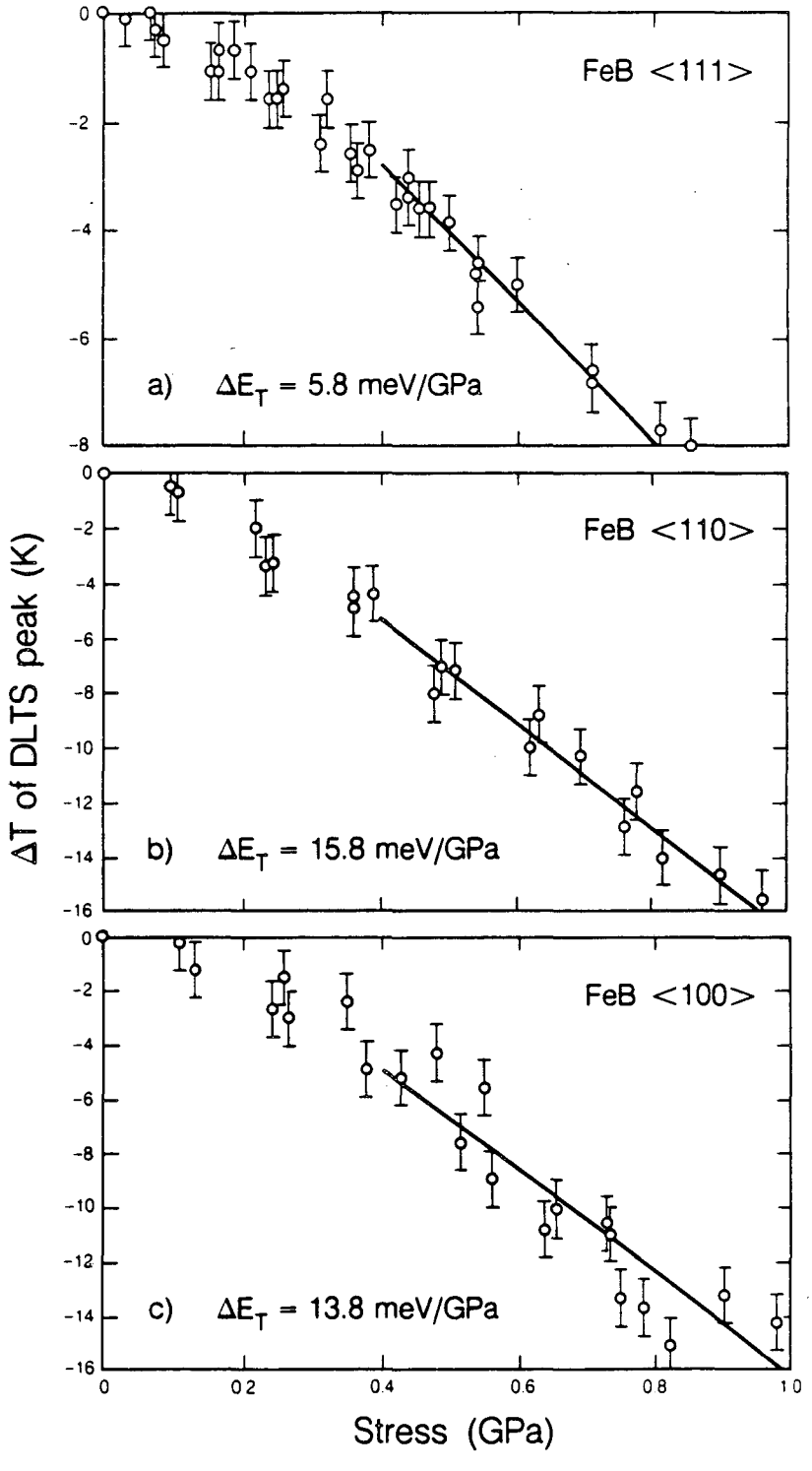

XBL 869-3557

Figure 3.

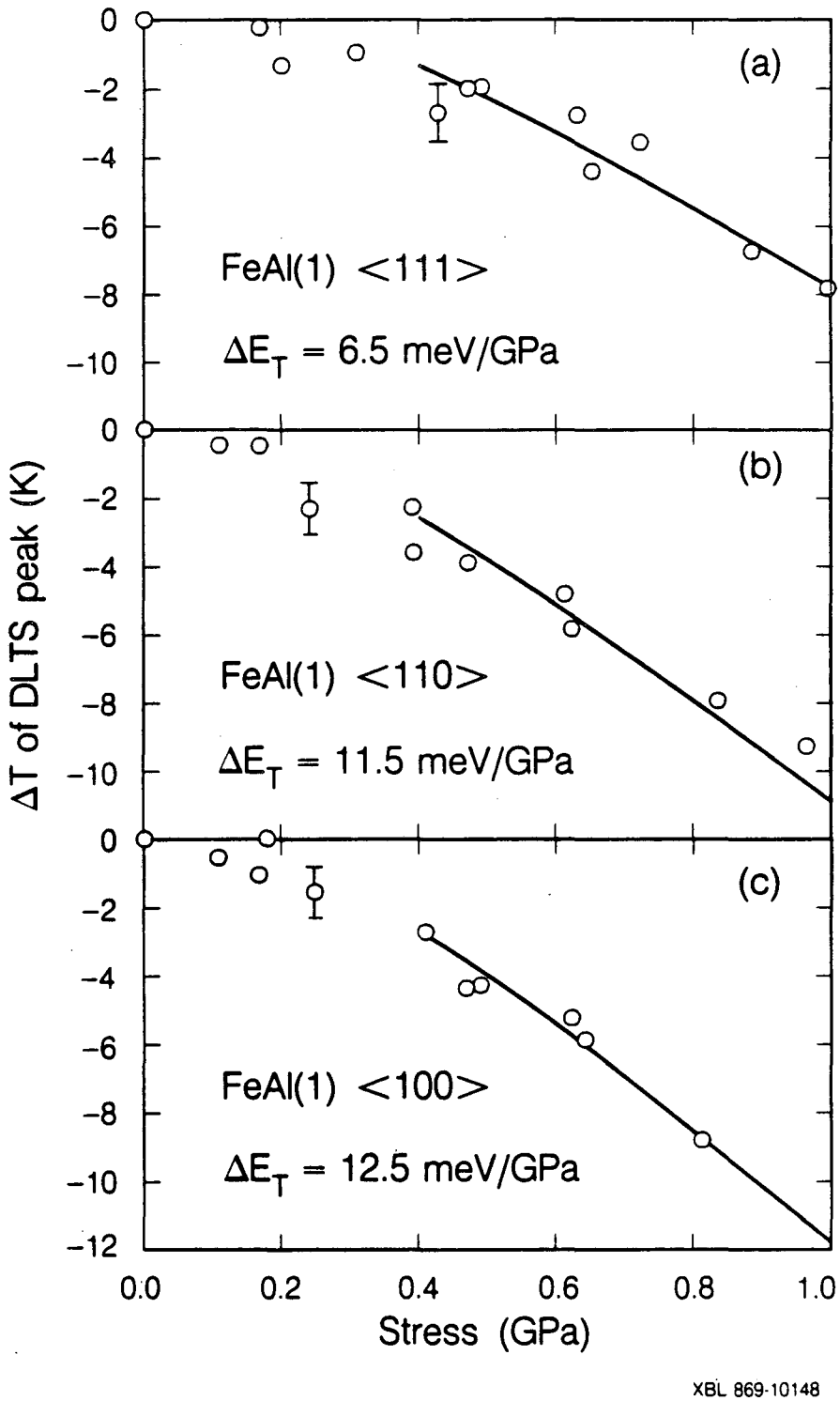
(a)
FeAl(1) <111>
ΔE_T = 6.5 meV/GPa
(b)
FeAl(1) <110>
ΔE_T = 11.5 meV/GPa
(c)
FeAl(1) <100>
ΔE_T = 12.5 meV/GPa
ΔT of DLTS peak (K)
Stress (GPa)
0
-2
-4
-6
-8
-10
-12
0.0
0.2
0.4
0.6
0.8
1.0
XBL 869-10148

Figure 4.

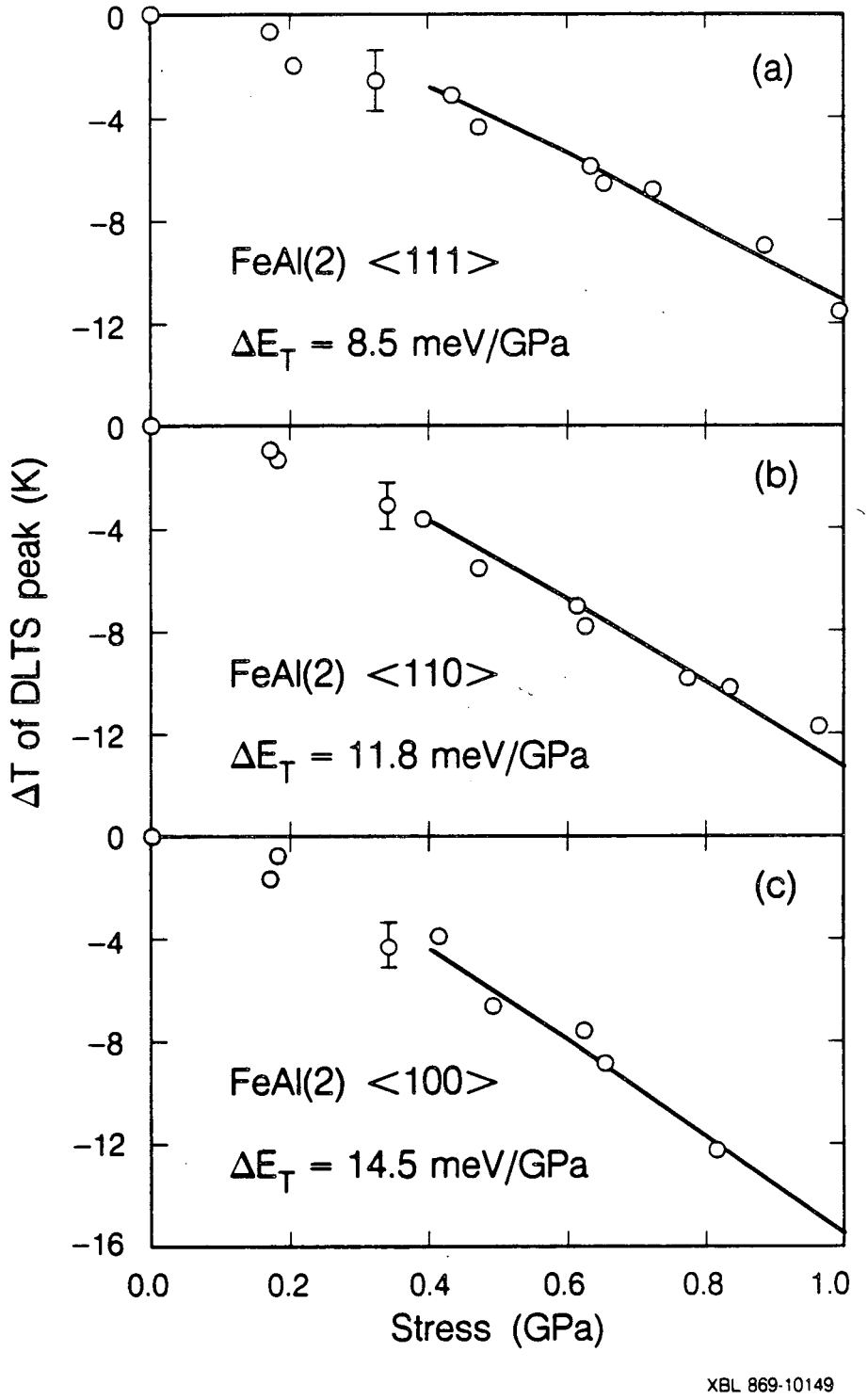
(a)
FeAl(2) <111>
ΔE_T = 8.5 meV/GPa
(b)
FeAl(2) <110>
ΔE_T = 11.8 meV/GPa
(c)
FeAl(2) <100>
ΔE_T = 14.5 meV/GPa
ΔT of DLTS peak (K)
Stress (GPa)
0
-4
-8
-12
-16
0.0
0.2
0.4
0.6
0.8
1.0
XBL 869-10149

Figure 5.

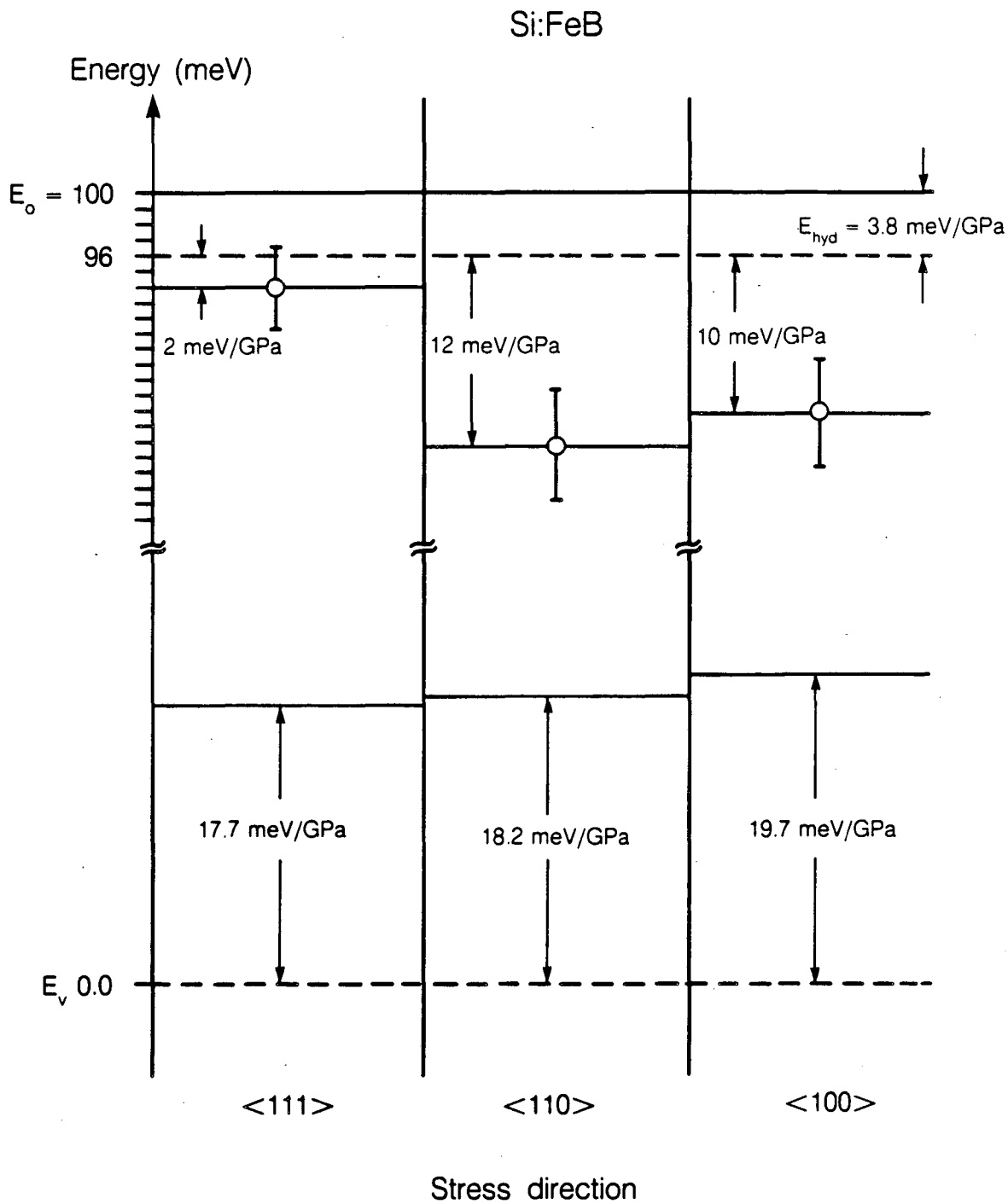

XBL 865-10111

Figure 6.

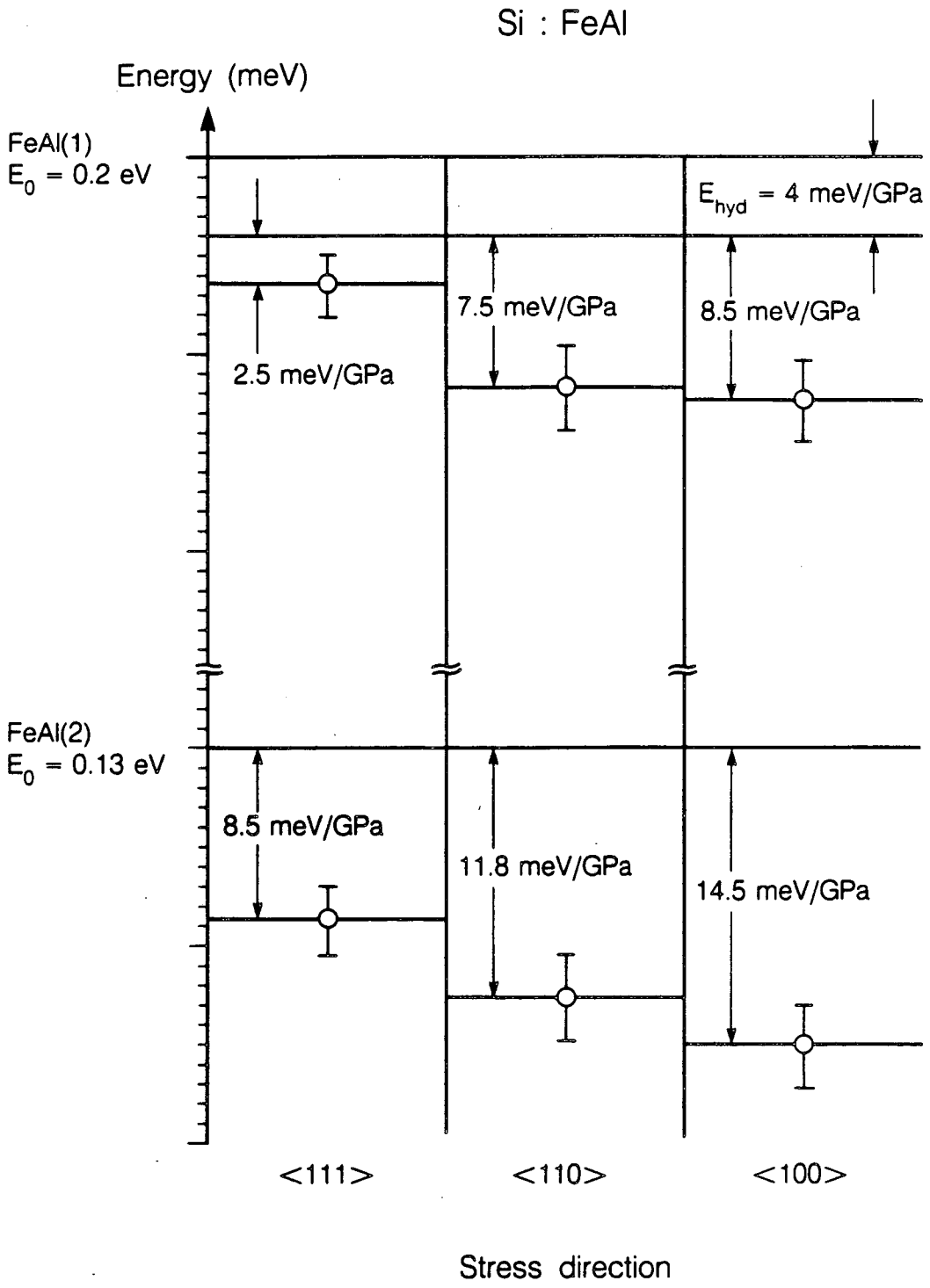

XBL 869-10147

Figure 7.

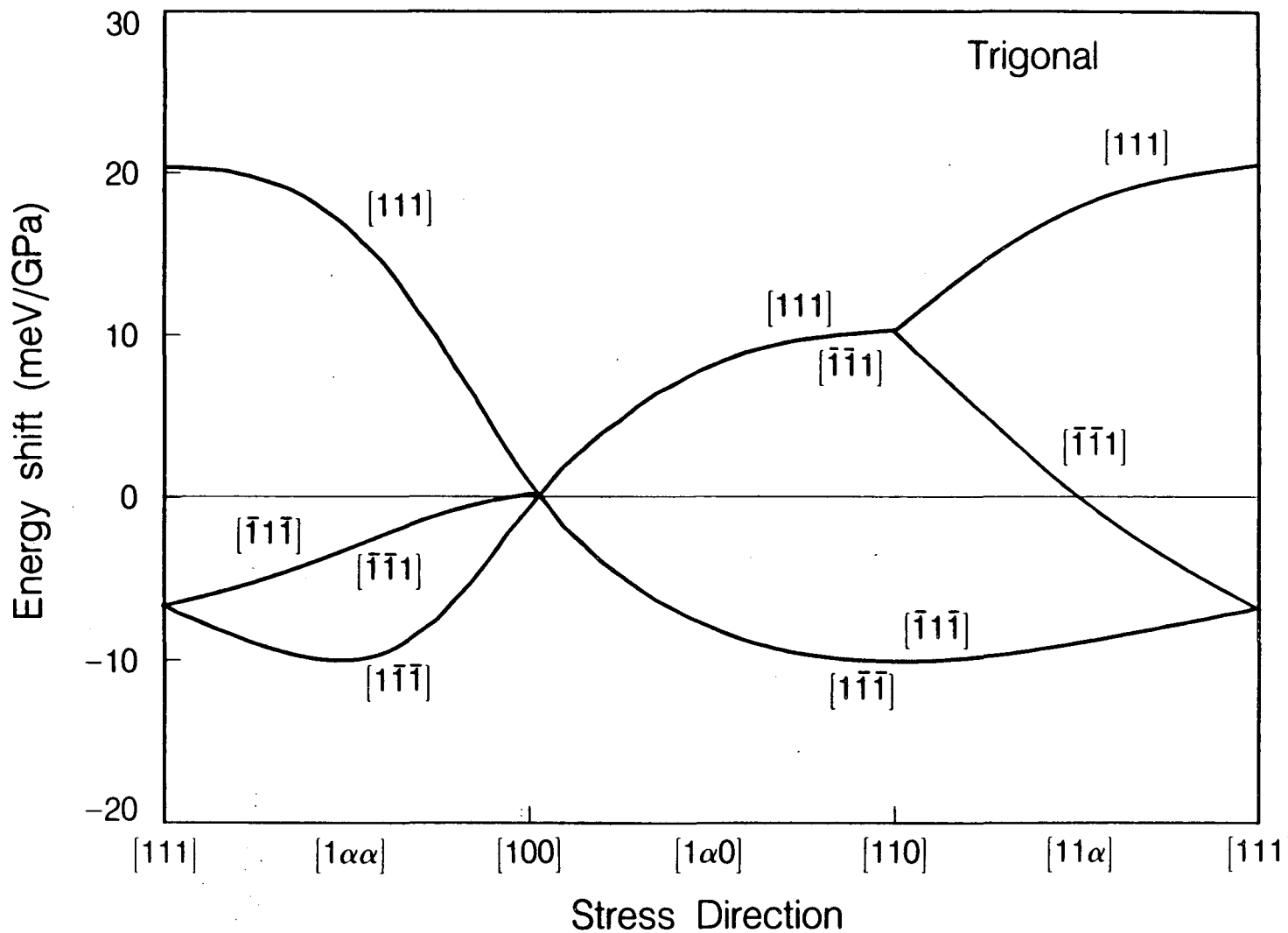

XBL 869-10146

Figure 8.

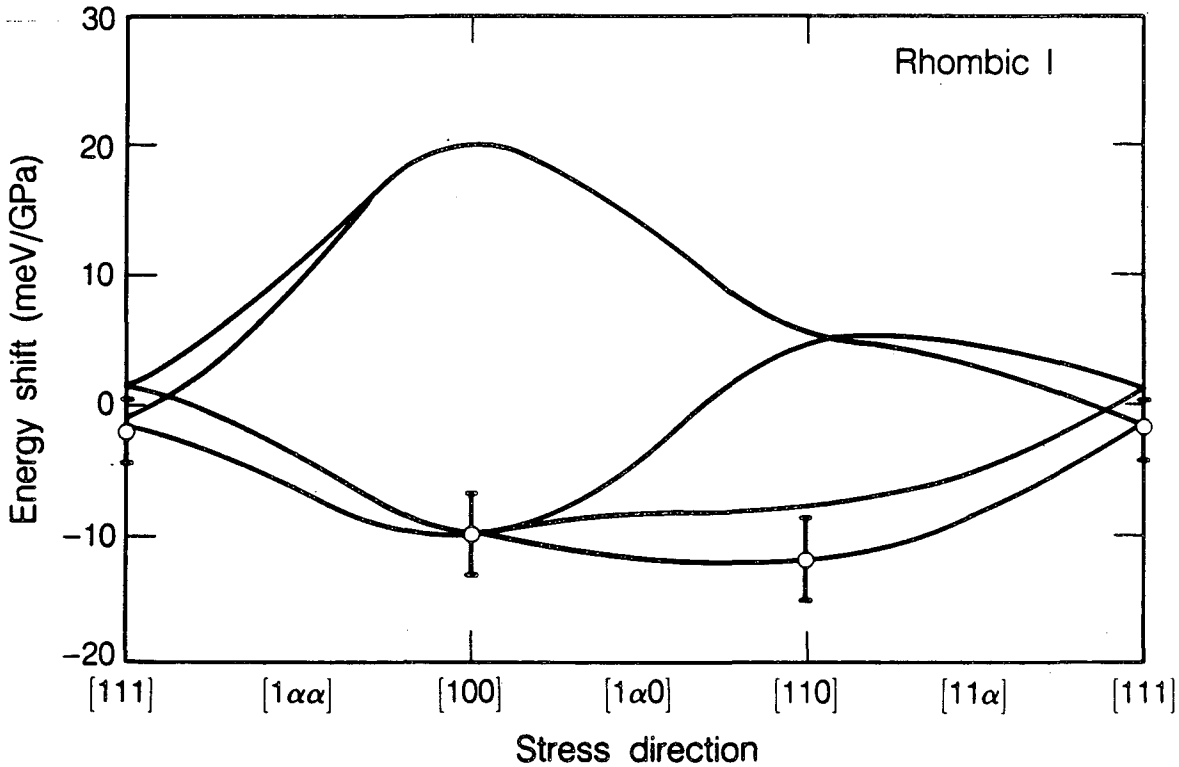

XBL 865-10143

Figure 9.

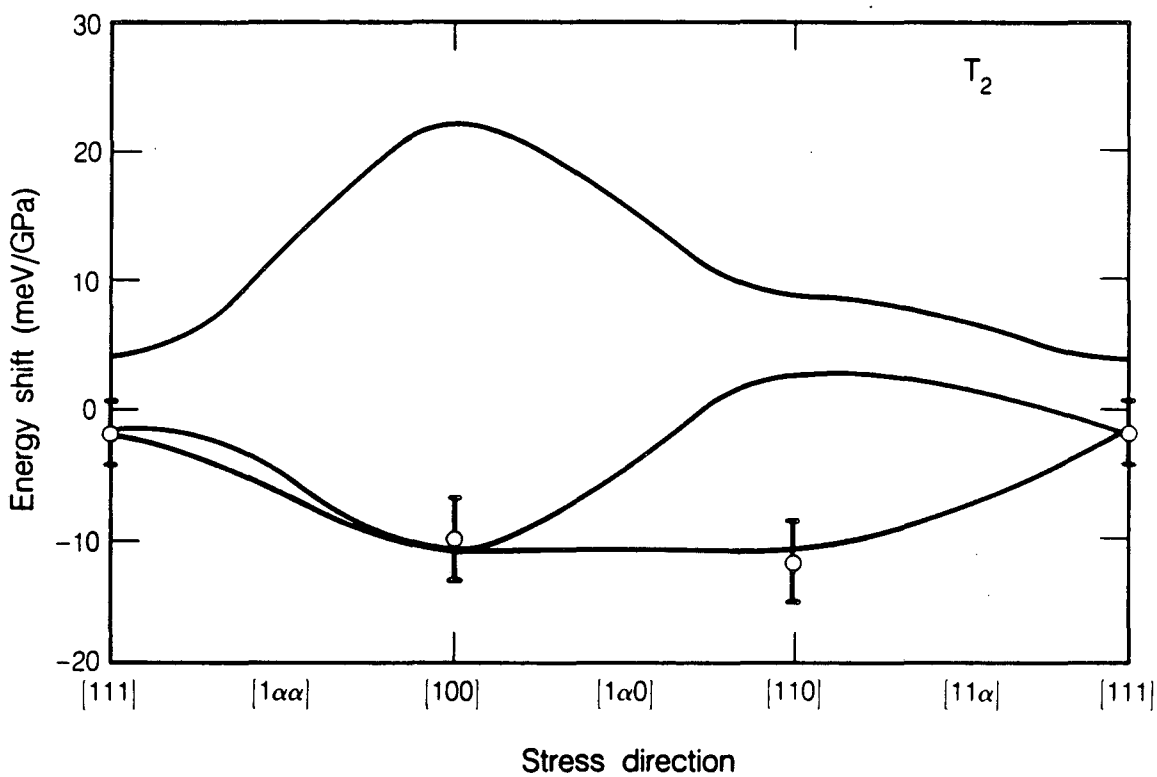

XBL 865-10142

Figure 10.

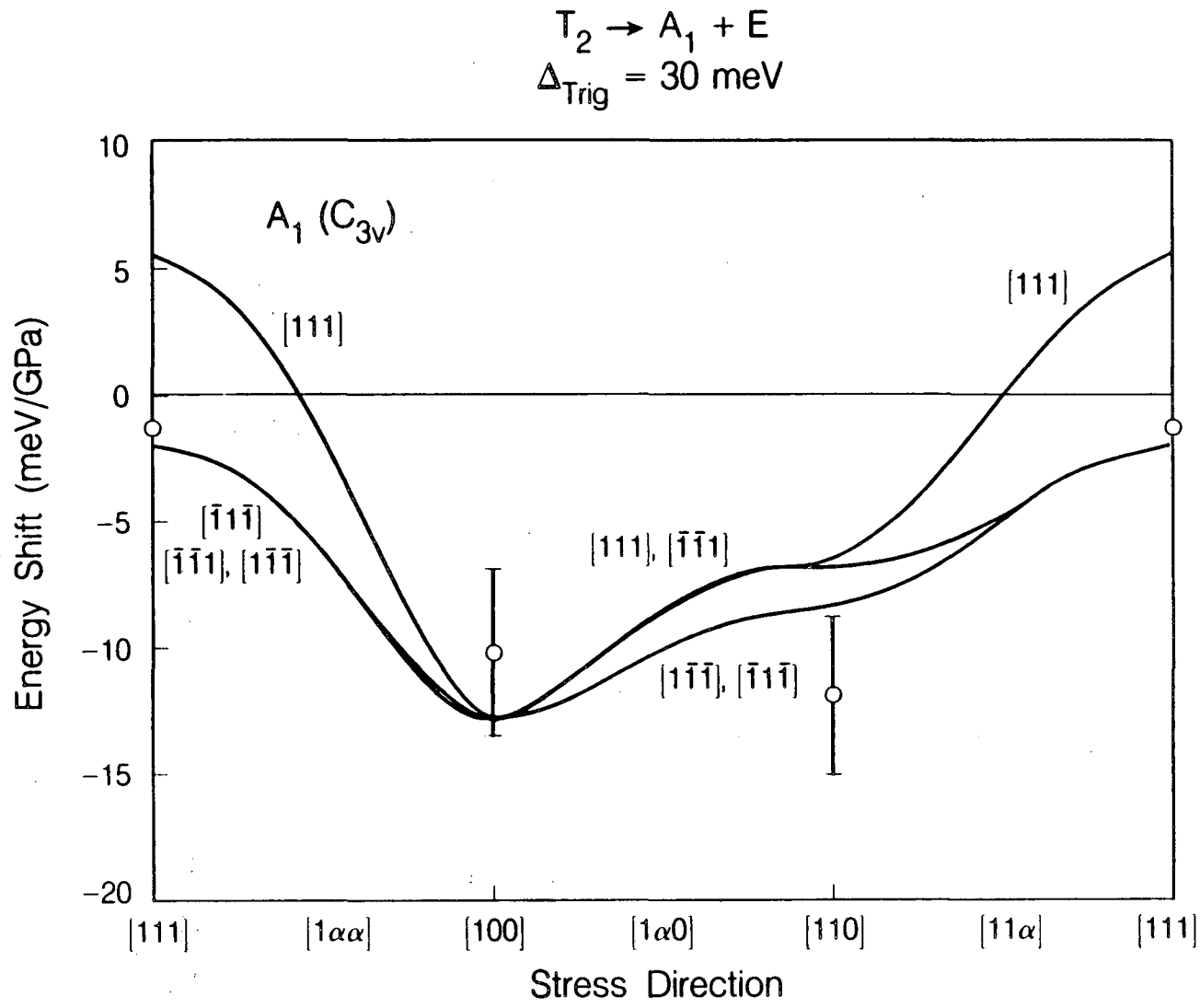

XBL 869-10144

Figure 11.

This report was done with support from the Department of Energy. Any conclusions or opinions expressed in this report represent solely those of the author(s) and not necessarily those of The Regents of the University of California, the Lawrence Berkeley Laboratory or the Department of Energy.

Reference to a company or product name does not imply approval or recommendation of the product by the University of California or the U.S. Department of Energy to the exclusion of others that may be suitable.

LAWRENCE BERKELEY LABORATORY
TECHNICAL INFORMATION DEPARTMENT
UNIVERSITY OF CALIFORNIA
BERKELEY, CALIFORNIA 94720